High-redshift star formation in the Hubble Deep Field revealed by a submillimetre-wavelength survey

David H. Hughes*, Stephen Serjeant†, James Dunlop*, Michael Rowan-Robinson†, Andrew Blain‡, Robert G. Mann†, Rob Ivison*, John Peacock*, Andreas Efstathiou†, Walter Gear§, Seb Oliver†, Andy Lawrence*, Malcolm Longair‡, Pippa Goldschmidt† & Tim Jenness‖

* Institute for Astronomy, University of Edinburgh, Royal Observatory, Edinburgh EH9 3HJ, UK
† Astrophysics Group, Imperial College, Blackett Laboratory, Prince Consort Road, London SW7 2BZ, UK
‡ Cavendish Astrophysics Group, Cavendish Laboratory, Madingley Road, Cambridge CB3 0HE, UK
§ Mullard Space Science Laboratory, University College London, Holmbury St Mary, Surrey RH5 6NT, UK
‖ Joint Astronomy Centre, 660 N. A'ohoku Place, Hilo, Hawaii 96720, USA

In the local Universe, most galaxies are dominated by stars, with less than ten per cent of their visible mass in the form of gas. Determining when most of these stars formed is one of the central issues of observational cosmology. Optical and ultraviolet observations of high-redshift galaxies (particularly those in the Hubble Deep Field) have been interpreted as indicating that the peak of star formation occurred between redshifts of 1 and 1.5. But it is known that star formation takes place in dense clouds, and is often hidden at optical wavelengths because of extinction by dust in the clouds. Here we report a deep submillimetre-wavelength survey of the Hubble Deep Field; these wavelengths trace directly the emission from dust that has been warmed by massive star-formation activity. The combined radiation of the five most significant detections accounts for 30–50 per cent of the previously unresolved background emission in this area. Four of these sources appear to be galaxies in the redshift range $2 < z < 4$, which, assuming these objects have properties comparable to local dust-enshrouded starburst galaxies, implies a star-formation rate during that period about a factor of five higher than that inferred from the optical and ultraviolet observations.

Recent years have seen the first meaningful attempts to determine the global star-formation history of the Universe, using the combined information provided by deep redshift surveys (for example, the Canada France Redshift Survey[1]) reaching $z \approx 1$, and the statistics of Lyman-limit galaxies[2] at higher redshifts in, for example, the Hubble Deep Field (HDF)[3–5]. The results[6] imply that the star-formation and metal-production rates were about 10 times greater at $z \approx 1$ than in the local Universe, that they peaked at a redshift in the range $z \approx 1$–1.5, and that they declined to values comparable to those observed at the present day at $z \approx 4$.

These conclusions, derived from optical-ultraviolet data, may however be misleading, because the absorbing effects of dust within distant galaxies undergoing massive star-formation may have distorted our picture of the evolution of the high-redshift Universe in two ways. First, the star-formation rate (SFR) in known high-redshift objects is inevitably underestimated unless some correction for dust obscuration is included in deriving the rest-frame ultraviolet luminosity. Second, it is possible that an entire population of heavily dust-enshrouded high-redshift objects, as expected in some models of elliptical galaxy formation[7], have gone undetected in the optical-ultraviolet surveys. The extent of the former remains controversial[8–11], while the possibility of the latter has until now been impossible to investigate.

Submillimetre cosmology

At high redshifts ($z > 1$), the strongly-peaked far-infrared radiation emitted by star-formation regions in distant galaxies is redshifted into the submillimetre waveband, and the steep spectral index of this emission on the long-wavelength side of the peak, at $\lambda \approx 100 \, \mu\text{m}$ in the rest-frame, results in a rapid increase in the rest-frame luminosity probed by submillimetre observations with increasing redshift, sufficient to offset the dimming of galaxies due to increasing cosmological distance. Consequently the flux density of a galaxy at $\lambda \approx 800 \, \mu\text{m}$ with fixed intrinsic far-infrared luminosity is expected to be roughly constant at all redshifts in the range $1 \leq z \leq 10$ (refs 12–14).

This ease of access to the young Universe has already been exploited through successful pointed submillimetre observations of known high-redshift sources including lensed objects (IRAS F10214+4724[15] and the Cloverleaf quasar[16]), radio galaxies[14,17,18] and quasars[19,20]. These studies have demonstrated the potential of submillimetre cosmology and have shown that in at least some high-redshift galaxies, dust-enshrouded star formation is proceeding at a rate of $\gg 100 \, M_\odot \, \text{yr}^{-1}$, substantially greater than the more modest star-formation rates (on average $\sim (1 - 5)h^{-2} M_\odot \, \text{yr}^{-1}$) displayed by Lyman-break galaxies[3]. (Here $M_\odot$ is the solar mass, and h is the normalized Hubble constant in units of $100 \, \text{km s}^{-1} \, \text{Mpc}^{-1}$).

With the recent commissioning of the sensitive submillimetre array camera SCUBA on the James Clerk Maxwell Telescope (JCMT)[21] it is now possible to conduct unbiased surveys[22] in this wavelength region and quantify the amount of star-formation activity in the young Universe by observing directly the rest-frame far-infrared emission from dust in high-redshift galaxies. Here we describe the first results from an ultra-deep submillimetre survey centred on the HDF.

A submillimetre survey of hidden star formation in the HDF

Recent ISOCAM observations of the HDF at 6.7 and 15 μm have confirmed that the strong evolution seen in the IRAS galaxy population at low redshifts[23,24] continues out to redshifts of the order of unity[25,26]. Such mid-infrared studies cannot, however, provide any constraints at higher redshift. In contrast an 850-μm survey is predicted to be completely dominated by sources at $z \geq 1$, and the number of detectable sources is very sensitive to the high-redshift evolution of the dusty starburst population. In particular, a SCUBA survey of the HDF complete to a flux density limit

$S_{850\,\mu m} > 2$ mJy would be expected to detect <0.1 galaxies if there is no cosmic evolution, <1 galaxy if the evolution mirrored the Madau curve[4], but at least 2 sources if the number density and luminosity of infrared starburst galaxies continued to evolve strongly out to $z \approx 2$, and substantially more sources with $z > 2$ if the population continued to evolve or stayed constant at higher redshifts[7,12,27–29].

We chose to centre this deep 850-μm survey on the HDF, not only because the SCUBA field of view of ~ 6 arcmin² is well matched to the area of the HDF, but also to maximize the possibility of finding optical/infrared/radio counterparts and redshifts for any submillimetre sources which were detected. Currently there exist over 20 spectroscopic redshifts for galaxies at $z > 2$ within the HDF, while the availability of deep photometric data[30] in the U_{300}, B_{450}, V_{606} and I_{814} bands facilitates the estimation of photometric redshifts for other galaxies in the field.

Simultaneous diffraction-limited images of the HDF at 850 and 450 μm were taken with SCUBA[21] on the 15-m JCMT. A total of 50 hours integration between 5 January and 13 February 1998 were centred at right ascension (RA) 12 h 36 min 51.2 s, declination (dec.) 62° 12′ 52.5″ (J2000) with occasional offsets 25 arcsec south, east and west to aid the discrimination of real and spurious sources. The data were taken under exceptional atmospheric conditions, with a median 850-μm sky opacity $\tau_{850\,\mu m} = 0.16$. Sky subtraction was performed using on-array chopping in RA in order to minimize the chop throw (important for accurate sky subtraction), to maximize the reclaimable signal-to-noise ratio for detected sources, and to minimize the number of negative off-beams arising from unknown sources well outside the primary field of view. We experimented with chopping in azimuth, but, at least at the declination of the HDF, this yielded no significant noise improvement over chopping in RA. Finally, to ensure that no significant source would be missed due to an unfortunate coincidence with the off-beam of another brighter source, the length of chop throw was varied, approximately half the observations (29 hours) adopting an RA chop-throw of 30 arcsec, and the remainder (21 hours) an RA chop-throw of 45 arcsec. As discussed below, this approach proved invaluable both for source confirmation, and for the separation of real and confused sources. The 850-μm data, with an angular resolution of 14.7 arcsec full-width at half-maximum (FWHM), covers an area of ~ 9 arcmin² and, due to the variation in the density of bolometer samples across the map, has a noise at the periphery approximately double its value at the map centre. The 850-μm image in Fig. 1 shows a circular field, within a radius of 100 arcsec from the map centre, and reaches a 1σ noise level of 0.45 mJy per beam. This image represents the deepest submillimetre map taken.

Submillimetre source extraction and confusion

Because the noise increases with radius from the map centre, sources were only sought within the central 80-arcsec radius of the image. The map shown in Fig. 1 displays 58 distinct peaks, most of which are noise. For gaussian filtered white noise, 1% of the peaks exceed 3.3σ in amplitude[31], and so a flux density of 1.5 mJy (at the map centre) is the practical detection threshold for real sources; the map contains 7 such objects. The use of two different chops and the effect of telescope nodding is to produce a convolving beam with four negative sidelobes. The signature of a source is therefore very different from noise, and this fact can be used to identify real sources and to deconvolve the map down to some flux density limit. Deconvolution also allows the flux in the sidelobes of a source to be reclaimed, thereby enhancing the signal-to-noise ratio of the detected sources. To investigate whether these peaks correspond to single, or blended, sources, simulations of random source distributions with plausible number counts have been performed. The 14.7-arcsec beam is sufficiently broad that an ideal noise-free map would in fact never contain more than ~ 20 peaks within the 5.6 arcmin² map, independent of the true density of sources. Alternatively, the

observed source density is about one source per 12 beam areas; both arguments indicate that source confusion must become important at the limit of our 850-μm map.

It is thus possible that at least some of the apparent sources in the map could consist of emission from more than one object, and this is a particular concern for the weaker sources with $S_{850\,\mu m} \approx 2$ mJy. One way of isolating such cases is optical identifications, as discussed below; if there is only a single candidate identification, the source cannot be a blend, as each member of the blend would have a separate optical counterpart.

Another approach is to note that confusion is only a serious problem when there is a blend of one or more sources of similar flux, and that in such cases the apparent source will usually be significantly broader than the telescope beam. This breadth means that the apparent source position will be less stable under the addition of noise than if the source is dominated by a single unresolved object. We have therefore taken the conservative approach of identifying sources in the full data set that appear in both the 30-arcsec and 45-arcsec chop images, and only keeping those whose positions agree to better than 3 arcsec. Tests on simulated source fields with realistic number counts show that this procedure should succeed in giving a clean sample of the sources brighter than 2 mJy in the central 80-arcsec radius of the image, each dominated by a single object. The positions of these 5 sources are given in Table 1, together with their 850-μm flux densities.

The simultaneous 450-μm image covers 75% of the useful area mapped at 850 μm and, despite the excellent observing conditions, which resulted in a 1σ r.m.s. noise signal of 7 mJy per beam at 450 μm, no significant detections were obtained.

Number counts and the submillimetre background

The map shown in Fig. 1 can be used to determine the form of the number counts at 850 μm fainter than the limit of 2 mJy at which
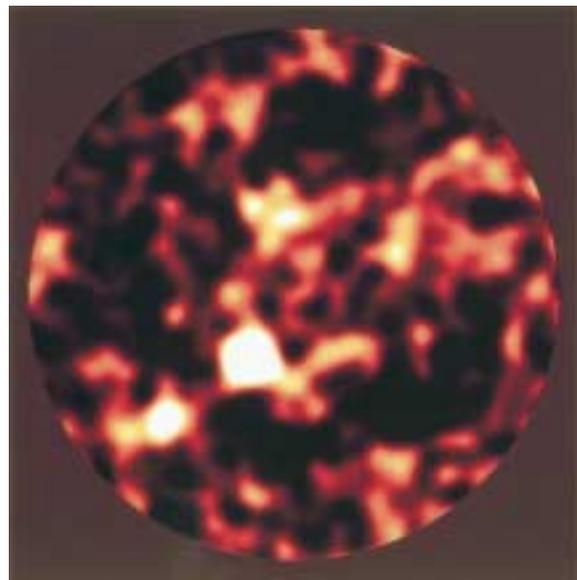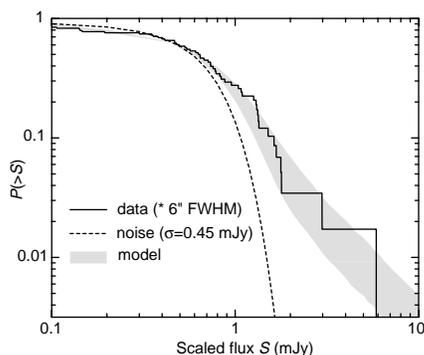

Figure 1 The 850-μm SCUBA image of the HDF. The image shows a radius of 100 arcsec from the map centre (RA 12 h 36 min 51.20 s, dec. +62° 12′ 52.5″; J2000) and is orientated with north upwards and east to the right. Primary flux calibration was performed using Uranus, with secondary calibration against a variety of AGB stars and compact H ɪɪ regions[54]. A signal-no-noise image is shown, allowing the significance of faint potential sources to be judged in a uniform manner, although it means there is a tendency for more sources to be detected in the central regions. The colour coding has been tuned so that the 5 most significant sources discussed here appear in white, while other formally significant flux-density peaks appear yellow. The absolute calibration uncertainty is $<10\%$. See Methods for details.

individual sources can be selected with some confidence. Fainter sources combine to raise the r.m.s. fluctuations in the map beyond what is expected purely from noise. There is a long tradition in radio and X-ray astronomy of extracting faint counts from such information using 'P(D)' analyses[32], although the present data set is unusual in that both random noise and confusion noise are of similar amplitude. The approach adopted here is to focus on the distribution of signal-to-noise ratios for the peaks of the map in Fig. 1 (that is, the distribution of fluxes for all apparent 'sources'). By generating synthetic maps with different number counts, it is possible to estimate what range of true counts is consistent with the observed distribution.

We have not explored the full parameter space, but some examples are illustrated in Fig. 2. Empirically, it is clear that there is an excess of peaks in the range 0.8–1.5 mJy, and this requires a substantial density of sources at about this flux-density level. The observed peak flux-density distribution is matched reasonably well by a source density of about 7,000 deg^{-2} brighter than 1 mJy, which corresponds to the observed density of brighter sources, extrapolated with a euclidean count slope, with the significant caveat that this number assumes an unclustered source distribution. If in fact the faint submillimetre sources are high-redshift starbursts, it is not implausible that they are strongly clustered on scales of several arcsec[33,34]. For a given surface density of sources, this increases the background fluctuations and so the above figure should probably be treated as an upper limit.

The counts must continue to flux densities somewhat fainter than 1 mJy, but the present data do not have the sensitivity to estimate where the inevitable break from the euclidean slope occurs. This is best constrained by asking at what flux density the extrapolated count exceeds the background. By summing the flux densities in Table 1, a lower limit to the background contributed by discrete sources of 20 mJy per 5.6 arcmin^2 is found, equivalent to $\nu I_\nu = 1.5 \times 10^{-10}\,\mathrm{W\,m^{-2}\,sr^{-1}}$, or approximately half the background estimate reported by Puget et al.[35] (where ν is the observing frequency and I_ν the specific intensity of the observed radiation at that frequency). There is, however, evidence in our data—specifically by continuing the deconvolution until the residual noise is statistically symmetric, or using the cumulative counts to 1 mJy derived above—that the true background contributed by discrete sources may be up to a factor of two higher than this, essentially

identical to the original estimate of Puget et al., and consistent with more than 50% of the revised background estimates at 850 μm (refs 36, 37) which suggest $\nu I_\nu = (5.0 \pm 4) \times 10^{-10}\,\mathrm{W\,m^{-2}\,sr^{-1}}$. The faint counts must therefore flatten by a flux density of ~0.3 mJy, otherwise even this background estimate would be exceeded.

Photometric observations and redshift estimation

Additional photometric observations during February 1998 at the centroid position of HDF850.1 confirmed the detection of the brightest submillimetre source with detections at 1,350 μm of 2.1 ± 0.5 mJy and at 850 μm of 7.0 ± 0.4 mJy. These data, together with a 450-μm 3σ upper limit of 21 mJy per beam, provide a robust photometric estimate of the redshift of the source. In Fig. 3 the expected flux density ratios at submillimetre and millimetre wavelengths are plotted as a function of redshift for a range of models, typical of dusty, star-forming galaxies, which are consistent with the observed optical to submillimetre spectra of Arp220, one of the most heavily enshrouded local starburst galaxies[38,39], and the high-z starburst/active galactic nucleus IRAS F10214+4724. The relevance of these models to galaxies in the high-z Universe is reinforced by noting that the measured submillimetre and millimetre wavelength flux-density ratios of known high-z objects[14,40] lie close to, or within the bounds of, the models.

The photometric redshift for HDF850.1, determined from the 1,350/850 μm flux-density ratio, lies within the range $2.5 < z < 9$.
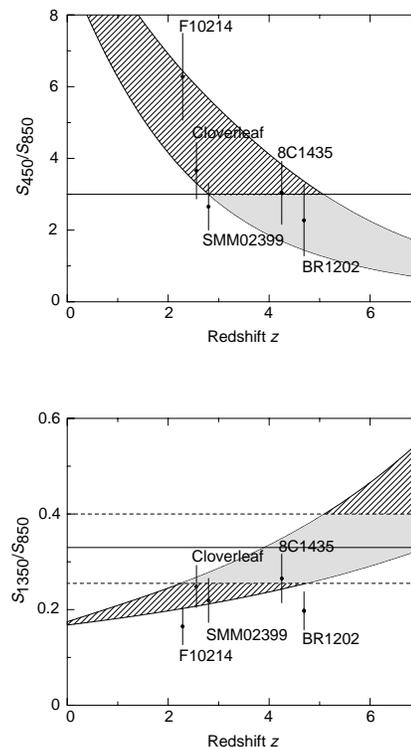

Figure 2 A comparison of observed and predicted number counts of submillimetre sources in the HDF as a function of flux density. The jagged solid line shows the raw integral number counts for the central 80-arcsec radius of the map in Fig. 1. The flux units here are signal-to-noise, but scaled to the flux units in the map centre. This uniform-noise representation allows a clear demonstration of sources in excess of the expectation for a pure noise field (dashed line) above ~0.8 mJy. Synthetic maps were made with the observed noise properties using a random distribution of sources having euclidean counts down to a limit of 0.3 mJy (although the results are insensitive to this cut-off). The grey band shows the effect of varying the integral surface density at 1 mJy between 4,000 and 10,000 degree^{-2}.

Figure 3 An estimation of redshift using the measured flux density ratio between wavelengths of 450 and 850 μm (top panel) and 1,350 and 850 μm (bottom panel). The hatched area in each plot shows the expected range of flux density ratio as a function of redshift bounded by two extreme models of dusty star-forming galaxies[38] (Arp220 and IRAS F10214+4724) which are consistent with observations of high-z galaxies[12,40]. The solid horizontal lines represent the measured flux ratios for HDF850.1 and, in the case of the $S(1,350\,\mu m/850\,\mu m)$ ratio, the horizontal dotted lines represent errors of $\pm 1\sigma$ on the observed ratio. The solid shading represents the parameter space satisfied by the photometric data for HDF850.1, including the non-detection at 450 μm, and illustrates that the redshift for HDF850.1 probably lies in the range $2.5 < z < 9$.

This strong constraint is supported by its non-detection at 450 μm which provides an upper limit to the 450/850 μm flux-density ratio and hence a lower limit to its redshift of $z > 3$. Less stringent, but similar, high-redshift limits can be estimated for all submillimetre sources detected in the HDF by arguing that their non-detection at 15 μm at a 3σ level of ~ 20 μJy (S. Oliver *et al.*, manuscript in preparation) implies a lower limit of $z \approx 2$ for sources at 850 μm brighter than 2 mJy, assuming a starburst galaxy model[38], or $z > 1.5$ assuming the observed spectral energy distribution (SED) of the extreme starburst galaxy Arp220. The radio far-infrared correlation[41] yields lower limits of $z = 1.75$ and $z = 2.75$ respectively for 2 mJy and 7 mJy sources detected at 850 μm, but not detected at 8.5 GHz (ref. 42) at a 5σ flux limit of 8 μJy. The above data demonstrate that deep submillimetre surveys provide an efficient means of identifying a population of star-forming galaxies at redshifts >2.

Optical associations with submillimetre HDF sources

Given the rest-frame optical/far-infrared ratios typical of luminous starburst galaxies, the high-redshift SCUBA-selected galaxies are not necessarily expected to be present in the optical HDF, despite its depth. Nevertheless, we briefly discuss in turn plausible associations
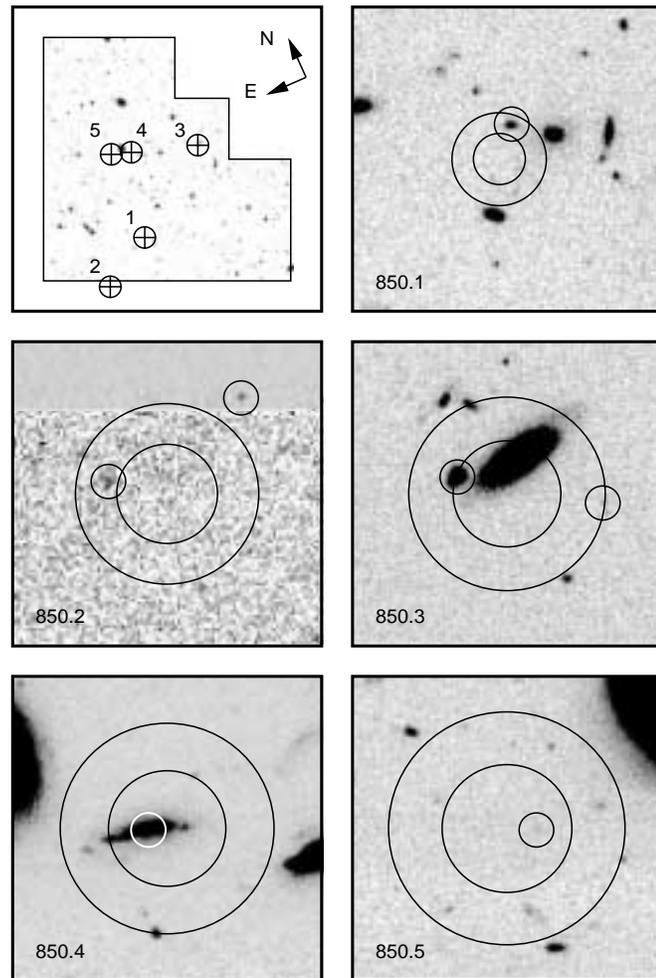
Figure 4 Optical associations for the brightest five submillimetre sources in the HDF. The top-left panel indicates the approximate location and orientation of each of the 10×10 arcsec I_{814}-band images shown in the following five panels. In each of these panels, the two large circles represent the 90% and 50% confidence limits on the submilimetre positional uncertainty, whilst a small circle (1 arcsec in diameter) has been used to mark the location of the most plausible optical association (or associations) for each SCUBA source (see text).

for the five most secure submillimetre sources in the HDF (see Fig. 4), estimating photometric redshifts[43], z_{ph}, for those galaxies without spectroscopic redshifts extended to include limits where galaxies are not detected in all four HDF bands.

Our approach is as follows. For each SCUBA source, we have considered as a potential optical counterpart all galaxies detected in the HDF whose distance from the SCUBA source lies within the 90% confidence limit of the submillimetre source position listed in Table 1. For each candidate we have then calculated the probability that a galaxy with such an optical magnitude (or brighter) could lie so close to the SCUBA position by chance, and also the probability that a galaxy with the observed redshift (or higher) could lie so close to the SCUBA position by chance. We note that these probabilities are often substantially higher than the raw Poisson probabilities[44]. This is due to the combined effect of the rather large uncertainty in the SCUBA positions, and the high surface density of galaxies at the limit of the optical HDF image, which together essentially guarantee that (with the exception of HDF850.1) every SCUBA source will have at least one optical identification candidate at the limit of the HDF image. Finally we have investigated whether any of the apparently most probable optical identifications can in fact be clearly rejected on the basis of the SED constraints discussed above.
HDF850.1. As shown in Fig. 4, this source lies 1.0 arcsec from galaxy 3–577.0 in the optical HDF catalogue[30] which has a tentative spectroscopic redshift of $z = 3.36$ (ref. 45), which has been claimed[46] to be gravitationally lensed by the foreground $I_{814}(AB) = 24$ elliptical galaxy 3–586.0 which lies at $1.0 \leqslant z \leqslant 1.2$ (refs 43, 47, 48) (where AB magnitude is as defined by Oke[49]). More recently, a 3.5σ detection (6.3 μJy) at 8.5 GHz has been associated with 3–586.0 (ref. 42). Based on its magnitude, the probability that 3–577.0 is a chance association with HDF850.1 is 0.33, while based on its redshift (which we estimate is $z_{ph} = 3.1$), the probability (calculated from the surface density of $z_{ph} > 3$ galaxies in photometric redshift catalogues[43,47,48]) is only 0.20. For 3–586.0 the probabilities are in fact comparable (0.29 and 0.49 respectively), but the non-detection of HDF850.1 at 15 μm ($S(3\sigma) < 23$ μJy) is strongly inconsistent (by almost two orders of magnitude) with the observed SEDs of any known galaxy (including Arp220) if placed at the 'low' redshift of 3–586.0, and as discussed above, the millimetre/submillimetre flux ratios also indicate that $z > 2.5$. Figure 5 shows that the observed spectrum of HDF850.1 agrees well with that expected for a starburst galaxy at redshift $z \approx 3$. We note that the random probability of being 2 arcsec from one of the radio sources[42] is only 0.03. If the radio source really is associated with 3–586.0, and HDF850.1 with 3–577.0, then these seemingly incompatible probabilities are best explained by assuming that 3–577.0 is indeed being gravitationally lensed by 3–586.0, thereby amplifying its rest-frame far-infrared flux, and increasing its chances of being detected at 850 μm by SCUBA. The amplification would, however, need to be fairly substantial to explain the statistics, implying a massive lens:

Table 1 Positions and flux densities for the five most reliable submillimetre sources in the HDF

Source	IAU name	RA (h min s)	Dec. (° ′ ″)	$S_{850\,\mu m}$ (mJY)
HDF850.1	J123652.3+621226	12 36 52.32 (±0.10)	+62 12 26.3 (±0.7)	7.0 ± 0.5
HDF850.2	J123656.7+621204	12 36 56.68 (±0.20)	+62 12 03.8 (±1.4)	3.8 ± 0.7
HDF850.3	J123644.8+621304	12 36 44.75 (±0.21)	+62 13 03.7 (±1.5)	3.0 ± 0.6
HDF850.4	J123650.4+621316	12 36 50.37 (±0.23)	+62 13 15.9 (±1.6)	2.3 ± 0.5
HDF850.5	J123652.0+621319	12 36 51.98 (±0.25)	+62 13 19.2 (±1.8)	2.1 ± 0.5

All these sources have $S_{850} > 2$ mJy. The positions of these sources (J2000) are reproduced from deconvolutions of both the 30-arcsec and 45-arcsec chopped images to within 3 arcsec. Positions given for each source were obtained from the average of the positions obtained using the independent SURF and IDL reductions. The quoted r.m.s. positional uncertainties were derived from the formula $\sigma_{pos} = \theta_{beam}/(2S/N)$, where θ_{beam} is the FWHM of the beam and S/N is the signal-to-noise ratio of the source. A further 0.5-arcsec uncertainty was added in quadrature, to account for the standard error in absolute pointing derived from measured pointing offsets throughout the observations. Flux densities quoted are the average from 3 independent methods, all of which agreed to within the formal uncertainty. Absolute calibration is uncertain to 10%.

3–586.0 may be the only visible member of a fainter group of galaxies.

HDF850.2 lies just beyond the edge of the HDF, making an assessment of possible optical associations difficult because the I_{814} band Hubble Flanking Field (HFF) image only reached a depth of ~25 mag. HDF850.2, however, is 4.3 arcsec from the $z_{ph} = 3.8$ galaxy 3–962.0 on the edge of the HDF, but based on its magnitude, the probability that 3–962.0 is a chance association with HDF850.2 is 0.63, while based on its redshift, the probability is 0.46. As can be seen in Fig. 4, there does appear to be a more convincing, but also very faint, candidate identification within the HFF, but at present we possess little useful colour information for this object. Therefore, although the non-detection at 15 µm implies a flux density ratio $S(850 \, \mu m/15 \, \mu m) > 190$ consistent with the SED of a starburst galaxy at $z > 2$, we are unable to make an unambiguous optical association.

HDF850.3 lies only 1.3 arcsec from 1–34.2 which is an asymmetric galaxy with $I_{814}(AB) = 24.5$ for which we estimate $z_{ph} \approx 1.95$. This is a moderately convincing identification, because, based on its magnitude, the probability that 1–34.2 is a chance association with HDF850.3 is only 0.29 (although based on its redshift the probability is 0.52) and its estimated redshift is consistent with a non-detection or marginal detection at 15 µm. The next nearest object is 1–34.0, a $I_{814}(AB) = 21$ galaxy at a distance of only 1.5 arcsec. For this galaxy, the random probabilities are 0.12 and 0.60, respectively, but with a tentative spectroscopic redshift of 0.49, and photometric redshift estimates in the range $0.26 \leqslant z_{ph} \leqslant 0.68$, this object can be confidently rejected as a possible identification given its non-detection at 15 µm, 450 µm, and radio wavelengths. We note also that 1–34.0 shows no obvious signs of starburst activity at optical wavelengths, and appears to be a relatively undisturbed spiral galaxy. Should the identification with 1–34.2 prove to be erroneous, we note for completeness that two $z_{ph} \approx 3.9$ galaxies, the nearer being 1–27.0 and the further being 1–31.0, lie within 4 arcsec of HDF850.3. Based on magnitude, the probability that these are chance associations is 0.63, while based on redshift, it is 0.3.

HDF850.4 lies less than 1 arcsec from 2–339.0, an $I_{814}(AB) = 23$ galaxy for which photometric redshifts have been determined in the range 0.74–0.88 (refs 43, 47, 48). This is a convincing identification because the probability (based on its magnitude) that 2–339.0 is a chance association with HDF850.4 is only 0.07 (based on its redshift, the probability is 0.44). Moreover, this is the one case for

which the 850-µm source can be plausibly associated with an ISOCAM detection at 15 µm, which yields a flux density ratio $S(850 \, \mu m/15 \, \mu m) \approx 16$. This is in fact exactly the value expected from the observed SED of Arp220 if placed at $z \approx 1$. This supports an identification with 2–339.0, and emphasizes the usefulness of constraining the redshift using the $S(850 \, \mu m/15 \, \mu m)$ ratio. Furthermore, we note that this optical galaxy is clearly disturbed, as would be expected for an extreme starburst galaxy, providing further circumstantial evidence that it is the correct optical identification. However, should this identification prove erroneous, we note that there are three galaxies (2–294.0, 2–315.0, 2–319.0) with $z_{ph} > 3$ within 3.5 arcsec of HDF850.4.

HDF850.5 is located in a sparsely populated region of the HDF, but is only 0.9 arcsec away from the $I_{814}(AB) \approx 29$ galaxy 2–426.0, for which we estimate a photometric redshift of $z_{ph} = 3.2$. This is a moderately convincing identification; based on its magnitude, the probability that it is a chance coincidence is 0.46, but based on its redshift, it is a more impressive 0.16. This high-redshift association is consistent with the lack of a 15-µm detection at that position, but we note the difficulty of estimating photometric redshifts for such faint HDF galaxies. Finally, we note that seven other faint ($I_{814}(AB) > 27.5$) galaxies lie within 3.5 arcsec of HDF850.5 (see Fig. 4), but these objects are significantly more likely to be chance coincidences, and in any case all also have photometric redshifts $z_{ph} > 2$.

In summary, HDF850.4 appears to be associated with a disturbed starburst galaxy at $z_{ph} \approx 1$, HDF850.3 with an asymmetric galaxy at $z_{ph} \approx 2$, and HDF850.1 and HDF850.5 have relatively unambiguous associations with HDF galaxies, both of which are at $z_{ph} \approx 3$. For HDF850.2 we find a possible identification within the HDF at $z \approx 4$, and an alternative (also faint) candidate in the HFF which can be reasonably expected to lie at $z > 2$. We note that we are clearly unable to rule out the possibility that the true optical counterparts of a few of these sources may be too faint for detection, even in the HDF.
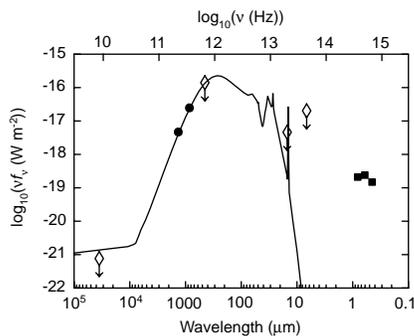
Figure 5 The observed optical–radio spectral energy distribution of HDF850.1. The filled circles represent the SCUBA 850- and 1,350-µm detections. Non-detections at 8.5 GHz (ref. 42), 450 µm (this work), 15 and 6.7 µm (S.O. *et al.*, manuscript in preparation) are shown as open diamonds. The filled squares indicate the optical fluxes in the I_{814}, V_{606} and B_{450} HST bands of the $z = 3.36$ galaxy 3–577.0, which is a plausible association for HDF850.1. A starburst galaxy model (solid curve)[38] has been redshifted to $z = 3.36$ and normalized to the 850-µm flux density. An additional radio non-thermal synchrotron component (where $F_\nu \propto \nu^{-0.8}$) is scaled to the starburst model at 60 µm using the radio/far-infrared correlation[41].
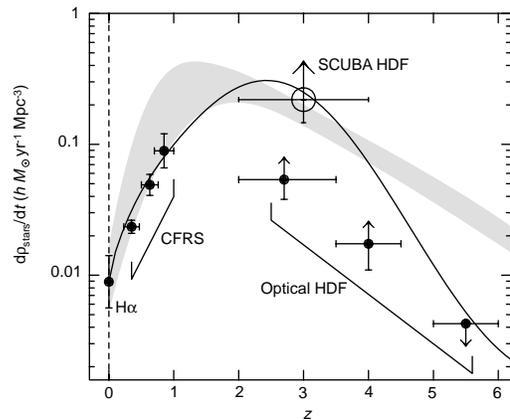
Figure 6 The global star-formation history of the Universe. Traditionally the mean co-moving rate of formation of stars in the universe, $d\rho_{stars}/dt$ has been measured from the total ultraviolet luminosity density of galaxies. At $z < 1$, this was measured by the Canada–France Redshift Survey of Lilly *et al.*[1], and at higher redshifts from the optical HDF data[3]. The zero-redshift datum was inferred from local emission-line galaxies[57]. The shaded region shows the prediction (assuming $h = 0.65$) due to Pei and Fall[53] who argued using the observed column densities in quasar absorbers, plus the low metallicities in these systems, that the star-formation rate must have peaked between $z = 1$ and $z = 2$. The solid line illustrates what would happen if the star-formation rate tracked the total output of radio-loud AGN[51]. Based on the evidence which indicates that four of the five brightest submillimetre HDF sources lie at $2 < z < 4$, we infer a rate ~5 times higher than that obtained by Madau[3], but in good agreement with the external predictions[51,52] of the rate at these epochs.

Dust masses and star-formation rates

The photometric redshifts and suggested optical identifications for the submillimetre sources are consistent with the expectation that all galaxies detected in the 850-μm survey of the HDF down to a flux limit $S_{850\,\mu m} = 2$ mJy should have redshifts $z \geqslant 1$. Given this, and the flat flux-density/redshift relation between $z = 1$ and $z = 10$, the dust-enshrouded SFRs and the dust masses for all five reliable sources can be estimated, independent of their precise redshifts. The results are given in Table 2, and indicate that these sources are extremely dusty and have SFRs, when determined from the submillimetre data, that are similar to, or exceed, that of the local ultra-luminous starburst galaxy Arp220. We note that the calculated SFRs are sensitive to the assumed stellar initial mass function (IMF) and stellar mass-range (and can, in the extreme increase and decrease by a factor of ~3). More striking is the comparison of the far-infrared SFRs with those calculated from the rest-frame ultraviolet luminosities. The far-infrared method gives SFRs on average a factor of ~300 larger. It has been shown that optical SFRs, estimated from Balmer emission-line luminosities in Lyman-break galaxies at $z \approx 3$, are larger than the ultraviolet SFRs by factors of 2–15. This upward correction, due to attenuation by dust[9,10], would still require a further factor of ~50 to explain the higher far-infrared SFRs. A similar situation has been observed in the local Universe where the ratio of far-infrared and Hα luminosities in ultra-luminous infrared starburst galaxies (ULIRGs) is ~60 times larger than that in disk galaxies[50], suggesting that in young starbursts most OB stars are still deeply buried in their opaque parent clouds. The submillimetre sources we have seen are then quite typical of local ULIRGs, but their relevance to the overall cosmic star-formation history depends on their space density.

The small uncorrected ultraviolet SFRs ($<1h^{-2}\,M_\odot\,\mathrm{yr}^{-1}$, Table 2) for the optical counterparts of the submillimetre sources are reasonable, given that these galaxies are typically a few magnitudes fainter in the rest-frame ultraviolet, possibly due to greater dust obscuration, than the population of Lyman-break galaxies at $z \approx 3.5$ which have SFRs of $\sim 2h^{-2}\,M_\odot\,\mathrm{yr}^{-1}$. Alternatively, it may be that the less-secure identifications are erroneous, and that some of the submillimetre sources may have true optical counterparts below the detection limit on the HST HDF image, and therefore probably at $z \geqslant 5$.

By summing the far-infrared SFRs and dividing by the appropriate cosmological volume, a first, conservative estimate of the level of dust-enshrouded star-formation rate in the high-redshift Universe can be made, using observations that are insensitive to the obscuring effects of dust. For illustrative purposes, it can be reasonably assumed that four of the five sources (all but HDF850.4) lie in the redshift interval $2 < z < 4$, in which case a lower-limit to the dust-enshrouded SFR density is $0.21h\,M_\odot\,\mathrm{yr}^{-1}\,\mathrm{Mpc}^{-3}$ (assuming an Einstein–de Sitter Universe) at $z \approx 3$. This datum is plotted in Fig. 6, where it can be compared with the optically derived star-formation history of the Universe[3,4], the dust-corrected star-formation history

predicted from the evolution of radio-loud active galactic nuclei[51] and that inferred from the metal-production rate as determined from the observed column densities and metallicities in absorbers[52,53] of radiation from quasars.

If the redshift distribution extended beyond $z = 4$, the mean redshift would increase, but due to increased cosmological volume the SFR density would decrease in such a way that the data would remain consistent with the curves shown in Fig. 6. For example, assuming a redshift range $2 < z < 5$ yields a star-formation density of $0.16h\,M_\odot\,\mathrm{yr}^{-1}\,\mathrm{Mpc}^{-3}$ at $z \approx 3.5$.

We emphasize that the SCUBA datum plotted in Fig. 6 is in fact rather robust. For example, should our proposed identification for HDF850.3 (1–34.2) prove to have a spectroscopic redshift significantly lower than $z = 2$, the effect on the data in Fig. 6 will be to lower the $z \approx 3$ SCUBA datum by only 20%. However, the effect of even one of these sources lying at still higher redshift is rather dramatic; if one of the 2–3 mJy submillimetre sources we have detected in fact lies at $z > 4$, this would yield a star-formation density of $0.1h\,M_\odot\,\mathrm{yr}^{-1}\,\mathrm{Mpc}^{-3}$ in the redshift range $4 < z < 6$, thus keeping the star-formation density essentially constant out to $z \approx 5$.

Finally, it is interesting to consider how the high-redshift star-formation density inferred from our submillimetre detections is altered by adoption of a much lower dust temperature (and hence much lower total far-infrared luminosity) than is displayed by ultra-luminous infrared starburst galaxies in the local Universe. The values of SFR given in column 5 of Table 2 have been derived using a starburst model of M82, and essentially identical numbers result from the adoption of a single dust temperature of 50 K. Nevertheless, it is certainly possible to reduce these values by up to a factor of ~10 if a single dust temperature of 20 K is adopted, and this would be sufficient to lower the $z = 3$ SCUBA datum plotted in Fig. 6 to a level consistent with the uncorrected star-formation density inferred from optical observations. However, such a situation must be regarded as extremely improbable for two reasons. First, it is highly unlikely that the most luminous far-infrared sources in the high-redshift Universe should have dust temperatures more comparable to that of the Milky Way than to all known luminous far-infrared galaxies. Second, while the adoption of such low dust temperatures reduces inferred SFR, it also inevitably results in much larger derived dust masses, >10 times larger than the values listed in Table 2. The inferred molecular gas masses in the $z \approx 3$ galaxies are then so large ($\sim 5 \times 10^{11}\,h^{-2}\,M_\odot$) that a star-formation density of $>0.5\,hM_\odot\,\mathrm{yr}^{-1}\,\mathrm{Mpc}^{-3}$ at higher redshift is then required to produce the necessary quantities of chemically enriched material[58]; reference to Fig. 6 shows that such a value would be ~100 times greater than the star-formation density at $z > 4$ inferred from optical observations. While such a discovery would be extremely exciting, this alternative interpretation of our data would seem very unlikely to be correct. In summary, adoption of an average dust temperature of 50 K for the brightest submillimetre sources in our survey is most consistent with all the available evidence, and does not require inferred star-formation densities at $z > 4$ which differ by orders of magnitude from the external predictions illustrated in Fig. 6.

The deep submillimetre survey of the HDF reported here demonstrates that a significant fraction (>80%) of the star-formation activity in the high-redshift Universe may have been missed in previous optical studies. Four of the five brightest submillimetre sources alone provide a density of dust-enshrouded star-formation at $z > 2$ which is at least a factor of ~5 greater than that deduced from Lyman-limit systems[3]. The extent to which even this is an under-estimate depends on the number of sources fainter than $S_{850} = 2$ mJy at comparable redshift.

Our survey has identified a population of high-redshift dusty starburst galaxies which contribute a significant fraction of the extragalactic background at 850 μm. These observations, together with complementary wider, shallower submillimetre surveys, are

Table 2 Star-formation rates and dust masses of the sources in Table 1

source	z_{est}	$\log_{10}L_{60\,\mu m}$ $(h^{-2}L_\odot)$	SFR $(h^{-2}M_\odot\,\mathrm{yr}^{-1})$		$\log_{10}M_{dust}$ $(h^{-2}M_\odot)$
			UV	FIR	
HDF850.1	3.4	12.15	0.7	311	7.88
HDF850.2	3.8	11.87	0.2	161	7.62
HDF850.3	2.0	11.76	2.0	127	7.52
HDF850.4	0.9	11.83	0.7	142	7.50
HDF850.5	3.2	11.64	0.3	95	7.36

Column 2, photometric redshifts based on the most probable optical associations. Column 3, 60-μm luminosity determined from the starburst model of M82[38] scaled to the observed 850-μm flux densities. Columns 4, 5, star-formation rates calculated from rest-frame ultraviolet (uv; 2,800Å) and far infrared (FIR; 60 μm) luminosities[3,26]. The UV flux densities at 2,800 Å are interpolated from the measured $I_{814}(AB)$ and $V_{606}(AB)$ magnitudes[30]. Column 6, dust masses, assuming β = 1.5, $T = 50$ K[15]. An Einstein–de Sitter cosmology is assumed.

now beginning to provide the first true measurement of the star-formation history for the early Universe, unhindered by the attenuating effects of dust. The challenge for the future is to follow up these observations, in particular those of the submillijansky sources which at present can only be detected statistically.

It is very possible that some of these submillimetre sources lie at $z > 5$, but demonstrating this will require the individual detection of these sources with sub-arcsec position errors. This will require both improved noise performance and higher spatial resolution in order to evade the confusion limit. Facilities such as the forth-coming generation of submillimetre arrays are ideally matched to these important programmes for astrophysical cosmology. □

Methods

The data, taken in jiggle-map mode, were reduced in parallel using two wholly independent methods. The first reduction used the SCUBA User Reduction Facility (SURF v1.2)[55], whilst the second reduction was performed with a specially-written IDL pipeline. Both methods incorporate individual bolometer r.m.s. noise weighting in the map reconstruction. An iterative temporal de-glitching and spatial sky subtraction was performed. The IDL maps were reconstructed using a noise-weighted "drizzling" technique[56] and were in excellent agreement with the independent SURF reconstructions. Individual subsets of the data were also reduced using both techniques, including the production of separate images with 30-arcsec and 45-arcsec chop throws. The centre of the map contains a higher density of bolometer samples than the periphery. Consequently, the noise is a function of position and this variation can be deduced exactly from the known jiggle pattern, and is approximated closely by a quadratic radial variation $\sigma \propto 1 + (r/90 \, \text{arcsec})^2$ in the central regions. In the SURF reduction, the noise has the statistical character of white noise filtered with a beam of FWHM 6 arcsec, with an r.m.s. of 0.65 mJy at the map centre. Convolution of the map reduces this noise, but possible confusion from faint sources means that it is preferable not to broaden the point-source response significantly. As a compromise, a further convolution with a 6-arcsec beam was applied, reducing the r.m.s. noise signal to 0.45 mJy at the map centre. The noise on the final map therefore has the character of white noise convolved with a beam of FWHM 8.5 arcsec. A signal-to-noise image is shown in Fig. 1, allowing the significance of faint potential sources to be judged in a uniform manner, although it means that there is a tendency for more sources to be detected in the central regions. The analysis of sources was restricted to the central 80-arcsec radius. Because the observing strategy yields a point-source response with negative sidelobes at 0.25 of the peak, the map was CLEANed and restored with a 14.7-arcsec FWHM gaussian beam.

1. Lilly, S. J., Le Févre, O., Hammer, F. & Crampton, D. The Canada-France redshift survey: the luminosity density and star formation history of the universe to $z \sim 1$. *Astrophys. J.* **460**, L1–L4 (1996).
2. Steidel, C. C. & Hamilton, D. Deep imaging of high redshift QSO fields below the Lyman limit: I. The field of Q0000-263 and galaxies at z = 3.4. *Astron. J.* **104**, 941–949 (1992).
3. Madau, P. et al. High-redshift galaxies in the Hubble Deep Field: colour selection and star formation history to $z \sim 4$. *Mon. Not. R. Astron. Soc.* **283**, 1388–1404 (1996).
4. Madau, P. The evolution of luminous matter in the universe. In *The Hubble Deep Field* (eds Livio, M. et al.) (STScI Symp. Ser., in the press).
5. Connolly, A. J., Szalay, A. S., Dickinson, M., SubbaRao, M. V. & Brunner, R. J. The evolution of the global starformation history as measured from the Hubble Deep Field. *Astrophys. J.* **486**, L11–L14 (1997).
6. Fall, S. M., Charlot, S. & Pei, Y. C. Cosmic emissivity and background intensity from damped Lyman-alpha galaxies. *Astrophys. J.* **464**, L43–L46 (1996).
7. Franceschini, A., Mazzei, P., De Zotti, G. & Danese, L. Luminosity evolution and dust effects in distant galaxies: implications for the observatiblity of the early evolutionary phases. *Astrophys. J.* **427**, 140–154 (1994).
8. Pettini, M., Smith, L. J., King, D. L. & Hunstead, R. W. The metallicity of high-redshift galaxies: the abundance of zinc in 34 damped Ly-α systems from z = 0.7 to 3.4. *Astrophys. J.* **486**, 665–680 (1997).
9. Pettini, M. et al. The spectra of star forming galaxies at high redshift. In *The Ultraviolet Universe at Low and High Redshift* (ed. Waller, W.) (AIP Press, Woodbury, New York, in the press).
10. Heckman, T. M., Robert, C., Leitherer, C., Garnett, D. R. & van der Rydt, F. The ultraviolet spectroscopic properties of local starbursts: implications at high-redshift. *Astrophys. J.* (submitted); also as preprint astro-ph/9803185 at ⟨http://xxx.lanl.gov⟩ (1998).
11. Meurer, G. R., Heckman, T. M., Lehnert, M. D., Leitherer, C. & Lowenthal, J. The panchromatic starburst intensity limit at low and high redshift. *Astron. J.* **114**, 54–68 (1997).
12. Franceschini, A., De Zotti, G., Toffolatti, L., Mazzei, P. & Danese, L. Galaxy counts and contributions to the background radiation from 1 micron to 1000 microns. *Astron. Astrophys. Suppl. Ser.* **89**, 285–310 (1991).
13. Blain, A. W. & Longair, M. S. Submillimetre cosmology. *Mon. Not. R. Astron. Soc.* **264**, 509–521 (1993).
14. Hughes, D. H., Dunlop, J. S. & Rawlings, S. High-redshift radio galaxies and quasars at sub-millimetre wavelengths: assessing their evolutionary status. *Mon. Not. R. Astron. Soc.* **289**, 766–782 (1997).
15. Rowan-Robinson, M. et al. The ultraviolet-to-radio continuum of the ultraluminous galaxy IRAS F10214+4725. *Mon. Not. R. Astron. Soc.* **261**, 513–521 (1993).
16. Barvainis, R., Antonucci, R., Hurt, T., Coleman, P. & Reuter, H.-P. The broadband spectral energy distributions of the Cloverleaf quasar and IRAS F10214+4724. *Astrophys. J.* **451**, L9–L12 (1995).
17. Dunlop, J. S., Hughes, D. H., Rawlings, S., Eales, S. A. & Ward, M. J. Detection of a large mass of dust in a radio galaxy at redshift z = 3.8. *Nature* **370**, 347–349 (1994).
18. Ivison, R. J. et al. Dust, gas, and evolutionary status of the radio galaxy 8C 1435+635 at z = 4.25. *Astrophys. J.* **494**, 211–217 (1998).
19. Isaak, K. G., McMahon, R. G., Hills, R. E. & Withington, S. Observations of high redshift objects at submillimetre wavelengths. *Mon. Not. R. Astron. Soc.* **269**, L28–L31 (1994).
20. Omont, A. et al. Continuum millimetre observations of high-redshift radio-quiet QSOs-II. Five new detections at $z > 4$. *Astron. Astrophys.* **315**, 1–10 (1996).
21. Holland, W. S. et al. in *Advanced Technology MMW, Radio, and TeraHertz Telescopes Proc. SPIE.* **3357** (in the press).
22. Smail, I., Ivison, R. J. & Blain, A. W. A deep sub-millimeter survey of lensing clusters: a new window on galaxy formation and evolution. *Astrophys. J.* **490**, L5–L8 (1997).
23. Saunders, W. et al. The 60-micron and far-infrared luminosity functions of IRAS galaxies. *Mon. Not. R. Astron. Soc.* **242**, 318–337 (1990).
24. Lawrence, A. et al. The QDOT all-sky IRAS galaxy redshift survey. *Mon. Not. R. Astron. Soc.* (submitted).
25. Oliver, S. J. et al. Observations of the Hubble Deep Field with the Infrared Space Observatory-III. Source counts and P(D) analysis. *Mon. Not. R. Astron. Soc.* **289**, 471–481 (1997).
26. Rowan-Robinson, M. et al. Observations of the Hubble Deep Field with the Infrared Space Observatory-V. Spectrla energy distributions, starburst models and star formation history. *Mon. Not. R. Astron. Soc.* **289**, 490–496 (1997).
27. Blain, A. W. & Longair, M. S. Observing strategies for blank-field surveys in the submillimetre waveband. *Mon. Not. R. Astron. Soc.* **279**, 847–858 (1996).
28. Pearson, C. & Rowan-Robinson, M. Starburst galaxy contributions to extragalactic source counts. *Mon. Not. R. Astron. Soc.* **283**, 174–192 (1996).
29. Hughes, D. H. & Dunlop, J. S. Continuum observations of the high-redshift universe at submillimetre wavelengths. In *Highly Redshifted Radio Lines* (eds Carilli, C. et al.) (ASP Conf. Ser., ASP, San Francisco, in the press).
30. Williams, R. E. et al. The Hubble Deep Field: observations, data reduction, and galaxy photometry. *Astron. J.* **112**, 1335–1389 (1996).
31. Bond, J. R. & Efstathiou, G. The statistics of cosmic background radiation fluctuations. *Mon. Not. R. Astron. Soc.* **226**, 655–687 (1987).
32. Condon, J. J. Confusion and flux-density error distributions. *Astrophys. J.* **188**, 279–286 (1974).
33. Steidel, C. C. et al. A large structure of galaxies at redshift $z \sim 3$ and its cosmological implications. *Astrophys. J.* (in the press); also as preprint astro-ph/9708125 at ⟨http://xxx.lanl.gov⟩ (1997).
34. Giavalisco, M. et al. The angular clustering of Lyman-break galaxies at redshift z = 3. *Astrophys. J.* (in the press); also as preprint astro-ph/9802318 at ⟨http://xxx.lanl.gov⟩ (1998).
35. Puget, J. L. et al. Tentative detection of a cosmic far-infrared background with COBE. *Astron. Astrophys.* **308**, L5–L8 (1996).
36. Fixen, D. J., Dwek, E., Mather, J. C., Bennett, C. L. & Shafer, R. A. The spectrum of the extra-galactic FIR background from the COBE IRAS observations. Preprint astro-ph/9803021 at ⟨http://xxx.lanl.gov⟩ (1998).
37. Guiderdoni, B., Bouchet, F. R., Puget, J. L., Lagache, G. & Hivon, H. The optically dark side of galaxy formation. *Nature* **390**, 257–259 (1998).
38. Rowan-Robinson, M. & Efstathiou, A. Multigrain dust cloud models of starburst and Seyfert galaxies. *Mon. Not. R. Astron. Soc.* **263**, 567–680 (1993).
39. Dudley, C. C. & Wynn-Williams, C. G. The deep silicate absorption feature in IRAS 08572+3915 and other infrared galaxies. *Astrophys. J.* **488**, 720–729 (1997).
40. Ivison, R. J. et al. A hyperluminous galaxy at z = 2.8 found in a deep submillimetre survey. *Mon. Not. R. Astron. Soc.* (in the press); also as preprint astro-ph/9712161 at ⟨http://xxx.lanl.gov⟩ (1998).
41. Sopp, H. M. & Alexander, P. A composite plot of far-infrared versus radio luminosity, and the origin of far-infrared luminosity in quasars. *Mon. Not. R. Astron. Soc.* **251**, 14P–16P (1991).
42. Richards, E. A., Kellermann, K. I., Fomalont, E. B., Windhorst, R. A. & Partridge, R. B. Radio emission from galaxies in the Hubble Deep Field. *Astron. J.* (submitted); also as preprint astro-ph/9803343 at ⟨http://xxx.lanl.gov⟩ (1998).
43. Mobasher, B., Rowan-Robinson, M., Georgakakis, A. & Eaton, N. The nature of the faint galaxies in the Hubble Deep Field. *Mon. Not. R. Astron. Soc.* **282**, L7–14 (1996).
44. Browne, I. W. A. & Cohen, A. M. Quasars near bright galaxies. *Mon. Not. R. Astron. Soc.* **182**, 181–187 (1978).
45. Zepf, S. E., Moustakas, L. A. & Davis, M. Keck spectroscopy of objects with lens-like morphologies in the Hubble Deep Field. *Astrophys. J.* **474**, L1–L5 (1997).
46. Hogg, D. W., Blandford, R., Kundic, T., Fassnacht, C. D. & Malhotra, S. A candidate gravitational lens in the Hubble Deep Field. *Astrophys. J.* **467**, L73–L75 (1996).
47. Sawicki, M. J., Lin, H. & Yee, H. K. C. Evolution of the galaxy population based on photometric redshifts in the Hubble Deep Field. *Astron. J.* **113**, 1–12 (1997).
48. Wang, Y., Bahcall, N. & Turner, E. L. A catalogue of colour-based redshift estimates for $z \lesssim 4$ galaxies in the Hubble Deep Field. *Astron. J.* (submitted); also as preprint astro-ph/9804195 at ⟨http://xxx.lanl.gov⟩ (1998).
49. Oke, J. B. Absolute spectral energy distributions for white dwarfs. *Astrophys. J. Suppl.* **27**, 21–35 (1974).
50. Leech, K. J. High-luminosity IRAS galaxies-II. Optical spectroscopy, modelling of starburst regions and comparison with structure. *Mon. Not. R. Astron. Soc.* **240**, 349–372 (1989).
51. Dunlop, J in *Observational Cosmology with the New Radio Surveys* (eds Bremer, M. N. et al.) 157–164 (Kluwer, Dordrecht, 1998).
52. Fall, S. M. & Pei, Y. C. Obscuration of quasars by dust in damped Lyman-alpha systems. *Astrophys. J.* **402**, 479–492 (1993).
53. Pei, Y. C. & Fall, S. M. Cosmic chemical evolution. *Astrophys. J.* **454**, 69–76 (1995).
54. Sandell, G. Secondary calibrators at submillimetre wavelengths. *Mon. Not. R. Astron. Soc.* **271**, 75–80 (1994).
55. Jenness, T. & Lightfoot, J. F. in *Astronomical Data Analysis Software and Systems VII* (eds Albrecht, R. et al.) 216–219 (ASP Conf. Ser. 145, ASP, San Francisco, 1998).
56. Hook, R. N. & Fruchter, A. S. in *Astronomical Data Analysis Software and Systems VI* (eds Hunt, G. & Payne, H. E.) 147 (ASP Conf. Ser. 125, ASP, San Francisco, 1997).
57. Gallego, J., Zamorano, J., Aragon-Salamanca, A., Rego, M. The current starformation rate of the local universe. *Astrophys. J.* **455**, L1–L4 (1995).
58. Eales, S. A. & Edmunds, M. G. The implications of large dust masses at high redshifts: a first look at galactic evolution in the submillimetre waveband. *Mon. Not. R. Astron. Soc.* **280**, 1167–1180 (1996).